Inorganic Chemistry

Article

pubs.acs.org/IC

Compression of Silver Sulfide: X-ray Diffraction Measurements and Total-Energy Calculations

David Santamaría-Pérez,*[,†,⊥] Miriam Marqués,[‡,⊥] Raquel Chuliá-Jordán,[†] José M. Menendez,[‡,⊥] Oscar Gomis,[§,⊥] Javier Ruiz-Fuertes,[∥,⊥] Juan A. Sans,[∥,⊥] Daniel Errandonea,[∥,⊥] and José M. Recio[‡,⊥]

[†]Departamento de Química Física I, Universidad Complutense de Madrid, 28040 Madrid, Spain

[‡]Departamento de Química-Física y Analítica, Universidad de Oviedo, 33007 Oviedo, Spain

[§]Centro de Tecnologías Físicas:Acústica, Materiales y Astrofísica, Universitat Politècnica de València, 46022 Valencia, Spain

[∥]Departamento de Física Aplicada-ICMUV, Universidad de Valencia, 46100 Valencia, Spain

Supporting Information

ABSTRACT: Angle-dispersive X-ray diffraction measurements have been performed in acanthite, Ag_2S, up to 18 GPa in order to investigate its high-pressure structural behavior. They have been complemented by ab initio electronic structure calculations. From our experimental data, we have determined that two different high-pressure phase transitions take place at 5 and 10.5 GPa. The first pressure-induced transition is from the initial anti-$PbCl_2$-like monoclinic structure (space group $P2_1/n$) to an orthorhombic Ag_2Se-type structure (space group $P2_12_12_1$). The compressibility of the lattice parameters and the equation of state of both phases have been determined. A second phase transition to a $P2_1/n$ phase has been found, which is a slight modification of the low-pressure structure (Co_2Si-related structure). The initial monoclinic phase was fully recovered after decompression. Density functional and, in particular, GGA+U calculations present an overall good agreement with the experimental results in terms of the high-pressure sequence, cell parameters, and their evolution with pressure.

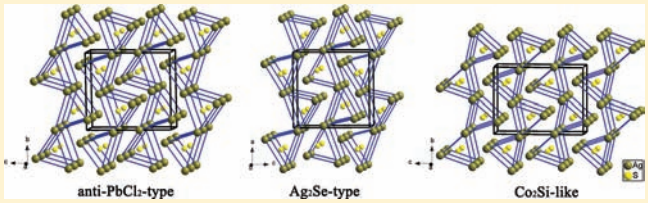

1. INTRODUCTION

Acanthite is the stable form of silver sulfide Ag_2S under ambient conditions,[1] which crystallizes in the monoclinic system, space group $P2_1/n$. It adopts an anticotunnite-like structure (anti-$PbCl_2$-like). The real cotunnite $PbCl_2$ structure is orthorhombic, space group *Pnma*, but slight distortions can be described using the monoclinic $P2_1/n$ space group. Due to its interesting electronic properties, Ag_2S has been used in semiconductor nanodevices, such as quantized conductance atomic switches, which would be good candidates for future solid-state memory devices.[2,3] Two other polymorphs of silver sulfide are known. (i) Upon heating above 176 °C, there is a phase conversion to a body-centered cubic form (space group $Im\bar{3}m$), referred to as argentite.[4−6] In this phase, the silver atoms are randomly distributed over the interstitial sites of a bcc sulfur lattice; this is the reason this HT phase has been considered as a possible ionic superconductor.[4,6] (ii) Further heating above 586 °C results in the conversion to a face-centered cubic polymorph.[4,5] However, the reliability of the existing powder diffraction studies on this latter high-temperature polymorph has recently been questioned.[7]

On the other hand, Ag_2S belongs to the family of M_2S binary sulfides that have recently also attracted renewed interest with respect to their HP behavior.[8−13] The completion of HP X-ray diffraction (XRD) measurements on the group IA sulfides up to 20 GPa revealed a common trend in their pressure-induced transformations. In particular, pressure drives structural changes from the antifluorite type through the anticotunnite type to the Ni_2In-type structures, a sequence that also occurs when the size of the M atom is increased. Therefore, the phase stability of these sulfides seems to depend on both the pressure and the relative atomic volumes.[10] This common trend should be, however, validated for other binary sulfides, such as those of group IB metals. Note that Mendeleev arranged the elements according to their chemical properties and placed silver (Ag) in the same column as alkali metals. Nevertheless, the electronegativity of silver (χ_{Ag} = 1.9) is considerably larger (χ_{Li} = 1.0, χ_{Cs} = 0.7);[14] this is the reason Ag_2S may be considered as formed by "covalent" bonds, instead of the "ionic" bonds existing in the alkali-metal sulfides. Therefore, its structural behavior could differ significantly from that of group IA sulfides.

The aim of this work is to study the structural stability of this compound under pressure in order to compare its behavior with that observed in alkali-metal sulfides and try to understand the existing differences. Room-temperature angle-dispersive X-ray diffraction (ADXRD) measurements were carried out up to 18 GPa using a diamond-anvil cell (DAC). The diffraction experiments allowed us to characterize two high-pressure phases, the transitions taking place at 5 and 10.5 GPa. First-principles calculations have complemented the experimental

Received: February 1, 2012
Published: April 24, 2012

   dx.doi.org/10.1021/ic300236p | *Inorg. Chem.* 2012, 51, 5289−5298

measurements, providing support and chemical insight into the observed behavior of Ag_2S under hydrostatic pressure.

2. EXPERIMENTAL AND THEORETICAL METHODS

2.1. Experimental Details. To perform X-ray powder diffraction measurements, commercial silver sulfide powder with 99.99% purity (Alfa Aesar, Prod. Nr. 12113) was crushed in a mortar with a pestle to obtain a micrometer-sized powder. Ambient-conditions X-ray diffraction confirmed that our sample has an anticotunnite-like structure.

Two independent high-pressure angle-dispersive X-ray diffraction experiments were conducted at room temperature. Experiment 1 was carried out up to 18 GPa with an Xcalibur diffractometer. X-ray diffraction patterns were obtained on a 135 mm Atlas CCD detector placed 110 mm from the sample using Kα molybdenum radiation (0.7107 Å). The X-ray beam was collimated to a diameter of 300 μm. The same setup was used previously to successfully characterize the high-pressure phases of other sulfides and oxides in the same pressure range.[9,10,15] Measurements were performed in a modified Merrill–Bassett diamond-anvil cell (DAC) with diamond culets of 450 μm. The diamond cell used for these experiments allows access to the angular range $4\theta = 50°$. The black Ag_2S powder was loaded in a 160 μm diameter hole of the stainless-steel gasket preindented to a thickness of about 50 μm. A 4/1 methanol/ethanol mixture was used as the pressure-transmitting medium. Exposure times were typically of 1 h duration. The CrysAlis software, version 171.34.49 (Oxford Diffraction Ltd.), was used for data collection and preliminary data reduction. Due to the appearance of the stainless-steel peaks of the gasket, only the high-pressure diffraction patterns below $2\theta = 18.3°$ are considered in this experiment.

Experiment 2, up to 17 GPa, was performed at the I15 beamline of the Diamond Light Source with an incident monochromatic wavelength of 0.4246 Å. The DAC and the sample loading were similar to those of experiment 1, with the exception of the pressure-transmitting medium used: a 16/3/1 methanol/ethanol/water mixture. The monochromatic X-ray beam was focused down to 30 × 30 μm using Kirkpatrick–Baez mirrors. A pinhole placed before the sample position was used as a cleanup aperture for filtering out the tail of the X-ray beam. The images were collected using a MAR345 image plate located 350 mm from the sample. Exposure times were typically 120 s. Preliminary data reduction was done using the Fit2D software.[16]

Ruby chips evenly distributed in the pressure chamber were used to measure the pressure in both experiments by the ruby fluorescence method.[17] Pressures measured in different ruby chips are within 0.1 GPa below 11 GPa and within 0.2 GPa at the maximum pressure of the experiments. The observed intensities were integrated as a function of 2θ in order to give conventional, one-dimensional diffraction profiles. The indexing and refinement of the powder diffraction patterns were performed using the FULLPROF[18] and POWDERCELL[19] program packages.

2.2. Computational Details. First-principles total-energy calculations were carried out within the DFT formalism with a plane-wave pseudopotential approach, as implemented in the Vienna ab initio simulation package (VASP).[20] We used the projector augmented wave (PAW) all-electron description of the electron-ion-core interaction.[21] Brillouin-zone integrals were approximated using the method of Monkhorst and Pack,[22] and the energies converged with respect to the k-point density ($12 \times 8 \times 8$ and $8 \times 12 \times 8$ meshes for the monoclinic $P2_1/n$ and orthorhombic $P2_12_12_1$ structures, respectively) and the plane-wave cutoff (420 eV). Initially, we used a conventional DFT exchange-correlation functional, within the generalized gradient approximation, the Perdew–Burke–Ernzerhof functional (PBE).[23] Transition-metal compounds such as Ag_2S experience strong intra-atomic exchange and Coulomb repulsion among the d electrons due to the many electrons and the localized, tight nature of the wave functions involved. Since DFT does not properly cancel out the electron self-interaction, the electron–electron repulsion is overestimated and, as a result, the electrons incorrectly delocalize to reduce the repulsion energy. In short, the covalency is overestimated.

To overcome the failure of DFT to describe the strongly correlated "d" electrons of Ag, the rotationally invariant form of DFT+U[24] was employed, where on-site Coulomb and exchange interactions as described in an unrestricted Hartree–Fock approximation are introduced to the DFT Hamiltonian. Within this approach, the Hubbard U, which is the Coulomb-energetic cost to place two electrons at the same site, and the approximation of Hund's exchange parameter J can be grouped into the single effective parameter U_{eff}. It can be understood as the introduction of a penalty function which disfavors noninteger occupation numbers of the on-site density matrix. It acts to reduce the one-electron potential locally for the Ag d orbitals, therefore reducing the hybridization with orbitals of the S atoms. To assess the strength of the correction, four values for U_{eff} have been used, namely 4, 5, 6, and 7 eV ($U_{eff} = 0$ case representing the DFT limit).

All structural relaxations were performed via a conjugate-gradient minimization of the total energy using the tetrahedron method with Blochl corrections.[25] We note that the calculated enthalpy vs pressure ($H(p)$) curves correspond to the static approximation (zero temperature and neglecting zero-point vibrational contributions).[26]

3. RESULTS AND DISCUSSION

3.1. Experimental Structural Study of Ag_2S. Figure 1 shows the ADXRD data for Ag_2S at several selected pressures in the two different experiments. Under ambient conditions, the X-ray diffraction pattern corresponds to the monoclinic anticotunnite-like structure previously reported (space group $P2_1/n$, No. 14)[1] with similar lattice parameters: $a = 4.2245(3)$ Å, $b = 6.9226(4)$ Å, $c = 7.8631(6)$ Å, and $\beta = 99.628(4)°$ ($Z = 4$, $V = 226.71(2)$ Å^3). This anti-$PbCl_2$-like structure is very common among the alkali-metal chalcogenides (both, at room and high pressure) and consists of trigonal prisms of Ag atoms connected by common edges forming chains which run parallel to the ab plane (see Figure 2a). The S atoms are located in the center of such prisms. Adjacent chains of prisms are shifted $1/2a$ along this axis (see Figure 2b). In fact, this $P2_1/n$ monoclinic distortion would correspond to the cation subarray of the β-Ca_2SiO_4 structure. A more detailed analysis of this structure type can be found in refs 8–10, 12, 13, and 27.

High-pressure X-ray diffraction patterns could be indexed in the initial monoclinic phase up to 4.7 GPa. For instance, the XRD pattern at 3.2 GPa (experiment 2) could be refined by the Rietveld method using the structural anti-$PbCl_2$ model (see Figure 3). The atomic coordinates of this structure are collected in Table 1. The obtained evolution for the unit cell volume and lattice parameters of the low-pressure (LP) phase of Ag_2S are shown in Figures 4 and 5a, respectively. There, it can be seen that the contraction of the lattice parameters is rather anisotropic.

dx.doi.org/10.1021/ic300236p | Inorg. Chem. 2012, 51, 5289–5298

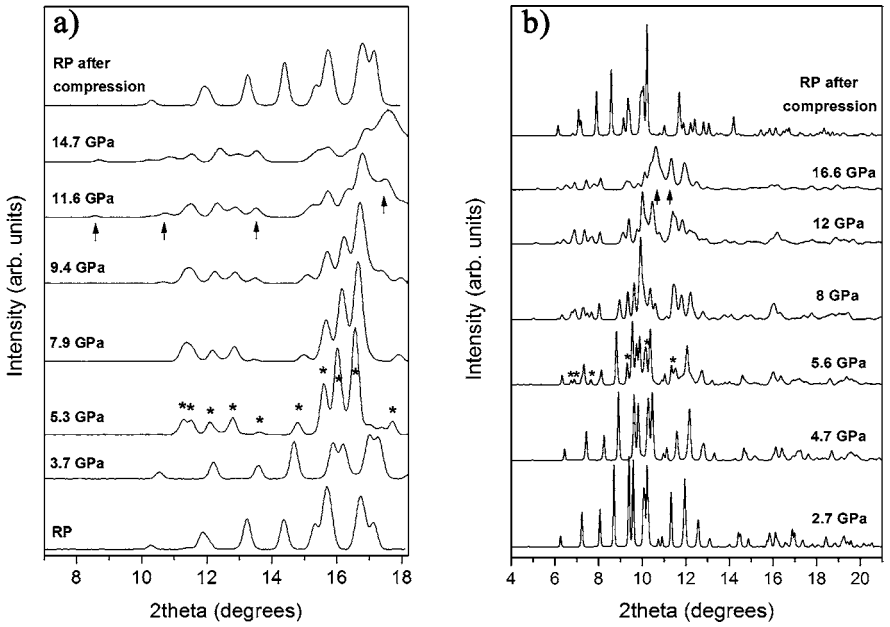

Figure 1. Selected X-ray powder diffraction patterns of Ag_2S without background. (a) Experiment 1, Xcalibur diffractometer, λ(Mo) = 0.7107 Å. The XRD patterns at 5.3 and 11.6 GPa clearly show the phase transitions to the first (HP1) and second (HP2) pressure-induced phases, respectively. Asterisks and arrows indicate diffraction peaks of the new phases. The upper pattern was taken under room conditions after the decompression process and shows the reversibility of the transitions. (b) Experiment 2, Diamond Light Source, λ = 0.4246 Å. The XRD patterns between 5.6 and 10.5 GPa show a coexistence of the initial LP phase and the HP1 phase (compare, for instance, the pattern at 8 GPa in this picture to that of 7.9 GPa in Figure 1a, corresponding strictly to the HP1 phase).

For instance, according to our experiments, the relative contractions for *a*, *b*, and *c* between room pressure and 4.7 GPa are 2.87, 4.05, and 0.57%, respectively. With regard to the values of the β angle, its variation is negligible up to 3.5 GPa and then the angle starts to decrease considerably with pressure (see Figure 5a). A third-order Birch–Murnaghan equation of state (EOS) was used to fit our pressure–volume data. By fixing the zero-pressure volume (V_0) to its measured value, we obtained the bulk modulus, B_0 = 38(2) GPa, and an unusually large value for the pressure derivative, B'_0 = 12(2). This large derivative is likely caused by a change in the compressibility of the LP phase of Ag_2S above 2.4 GPa. Therefore, we would have two different areas of compressibility. (i) Initially, the structure is highly compressible due, in particular, to the contraction of the sulfur polyhedra. The height of the [Ag_6] trigonal prisms is drastically reduced, whereas the nearest Ag–Ag distances (<4 Å) remain nearly constant. (ii) Above 2.4 GPa, the atomic positions are more stable and all the interatomic distances decrease at a slower pace. These two different compressibility regimes become evident on looking at the cell volume compression. Thus, at 2.33 GPa, the volume reduces 4.64%, whereas at 4.7 GPa the volume has only decreased 7.34% (2.7% more).

3.2. First Pressure-Driven Phase Transition. Upon further compression additional diffraction peaks appear and, in the case of experiment 1, the peaks of the low-pressure phase almost disappear at 5.4 GPa (see Figure 1a). This clearly indicates the existence of a structural phase transition at this pressure. At 6.9 GPa, the new diffraction peaks could be indexed in an orthorhombic cell with lattice constants *a* = 6.7249(12) Å, *b* = 4.1479(12) Å, and *c* = 7.2945(11) Å (*Z* = 4, *V* = 203.48(8) Å^3). Therefore, this structure implies a volume change of about 1.3% at the transition. The systematic absences in the indexed lattice planes are consistent with symmetry elements (screw axes) of the space group $P2_12_12_1$. This space group is also adopted by the mineral naumannite, Ag_2Se, at ambient conditions.[28−30] Therefore, we used the structural model of silver selenide to refine the X-ray diffraction patterns by the Rietveld method above 5.4 GPa, leading to the lattice constants and atomic parameters collected in Table 1 (XRD pattern at 6.9 GPa). This X-ray diffraction pattern is shown in Figure 6 together with the calculated and difference profiles to illustrate the quality of the refinement. The refined parameters were the overall scale factor, the cell parameters, the pseudo-Voigt profile function with terms to account for the reflection anisotropic broadening, and the fractional atomic coordinates. The background was manually subtracted and not refined. During the refinement process, displacement factors were physically meaningless, and for this reason, the overall displacement parameter was fixed to 0.1 Å^2. This high-pressure phase will be henceforth referred to as the HP1 phase.

This HP1 structure, depicted in Figure 2c, is basically a significantly distorted form of the initial anticotunnite-like phase. It can be described in a similar way as composed of chains of trigonal prisms formed by Ag atoms connected by common edges, each of these prisms being centered by a S atom. Adjacent chains of prisms are shifted by approximately 1/2*b* along this axis. However, in this case, these chains are no longer running parallel to each other. The lattice transformation entails a small displacement of the atoms in such a way that the chains of trigonal prisms are tilted with respect to the adjacent ones (see Figure 2d). However, the coordination number of the atoms does not change at the phase transition. The rectangular faces of the [Ag_6] prisms are capped by three additional Ag atoms belonging to adjacent chains so that the coordination number of the S atoms remains 8 + 1 (see Table 2). With regard to the Ag atoms, there are two crystallographically distinct Ag atoms in the orthorhombic unit cell. One Ag atom (Ag2) is surrounded by four S atoms in a

dx.doi.org/10.1021/ic300236p | *Inorg. Chem.* 2012, 51, 5289−5298

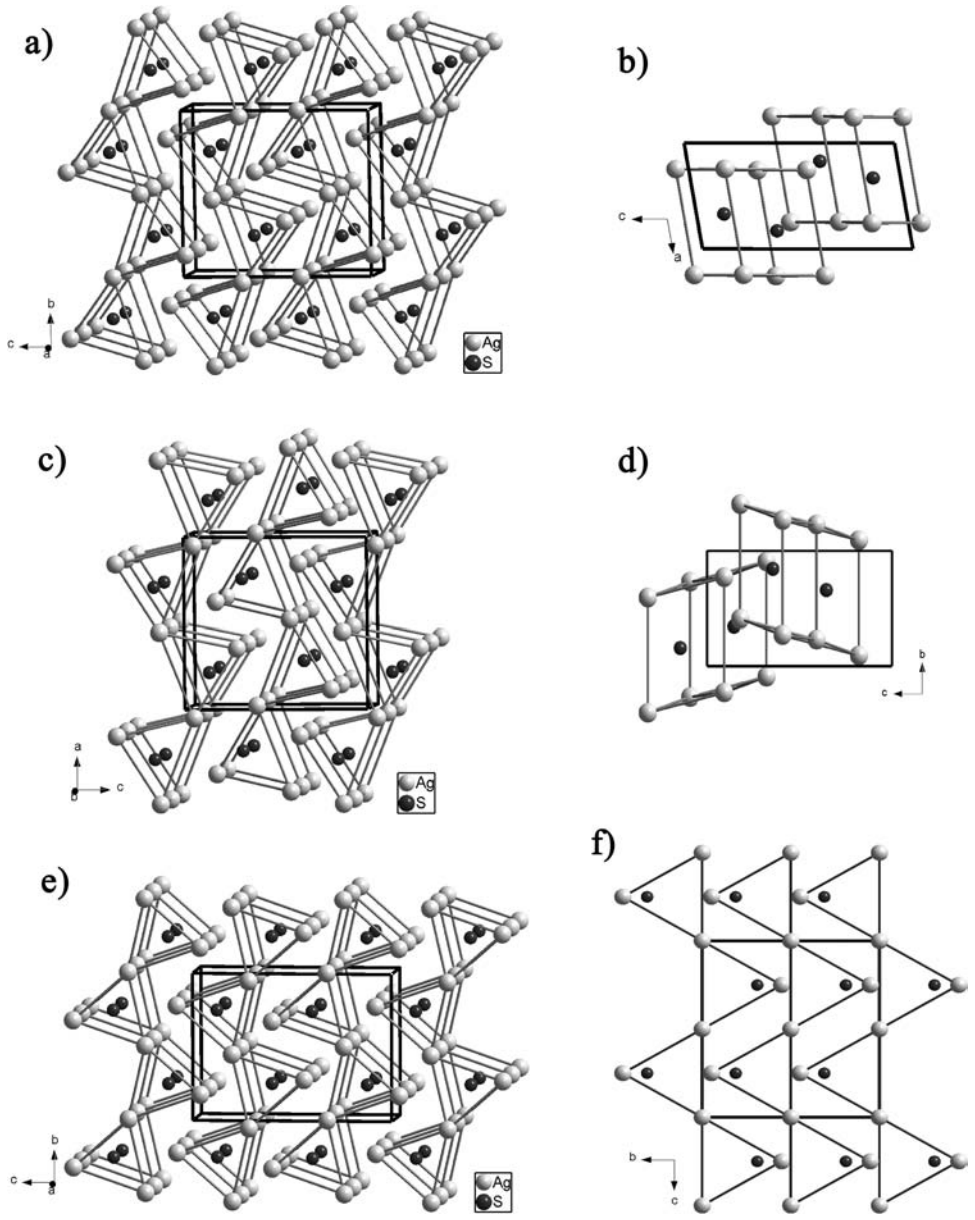

Figure 2. (a) Anticotunnite-like structure of the low-pressure $P2_1/n$ phase of Ag_2S at 3 GPa. (b) Projection of this LP phase along the *b* axis, showing that adjacent chains of prisms are shifted 1/2*a* and are parallel. (c) Ag_2Se-type structure of the HP1 $P2_12_12_1$ phase of Ag_2S at 6.9 GPa. (d) Projection of this HP1 phase along the *a* axis, showing that adjacent chains of prisms are shifted 1/2*b* and are tilted with respect to each other. (e) Anticotunnite-like structure of the HP2 $P2_1/n$ phase of Ag_2S at 16.5 GPa. (f) Projection along the *a* axis of the theoretically predicted *Cmcm* phase for Ag_2S at low pressures.

distorted-tetrahedral coordination (distances ranging from 2.25 to 3.13 Å), while the second Ag atom (Ag1) exhibits a 5-fold coordination defined by four S atoms forming a rectangular face and another S atom that completes the square pyramid (distances ranging from 2.6 to 3.16 Å).

A different behavior is observed in the experiment carried out with synchrotron radiation. In experiment 2, the initial monoclinic $P2_1/n$ phase coexists with the $P2_12_12_1$ orthorhombic phase from 5 GPa up to 10.5 GPa (see Figure 1b). This fact must be due to a slight change in loading parameters, i.e. the ratio between the amount of sample and pressure medium loaded, which would drive the transition to not occur completely. In any case, the quality of the XRD patterns allows us to obtain the values of the lattice constants of the HP1 structure in the pressure range 5−10 GPa (Figure 5b).

The equation of state and the pressure evolution of the lattice parameters of the HP1-Ag_2S phase are shown in Figures 4 and 5b, respectively. It can be seen that, in this HP1 phase, the *c* axis is the most compressible of the lattice constants and the *b* axis is almost incompressible. The linear compressibilities of the different axes are $\kappa_a = 0.015(2)$ GPa^{-1}, $\kappa_b = 0.0002(18)$ GPa^{-1}, and $\kappa_c = 0.0409(19)$ GPa^{-1}, which show the anisotropic compression of the orthorhombic unit cell. This anisotropy is related to the relative tilting of the $[Ag_6S]$ trigonal prisms which causes the Ag atoms to be located very close to each other along the *b* direction (distances between 2.61 and 2.88 Å at 6.9 GPa vs distances >2.92 Å in the monoclinic structure at 4.7 GPa). Consequently, it is quite likely that the cationic repulsion causes the incompressibility of this axis. A third-order Birch−Murnaghan equation of state was fitted to the variation of the unit cell volumes of the HP1 phase with pressure.

dx.doi.org/10.1021/ic300236p | *Inorg. Chem.* 2012, 51, 5289−5298

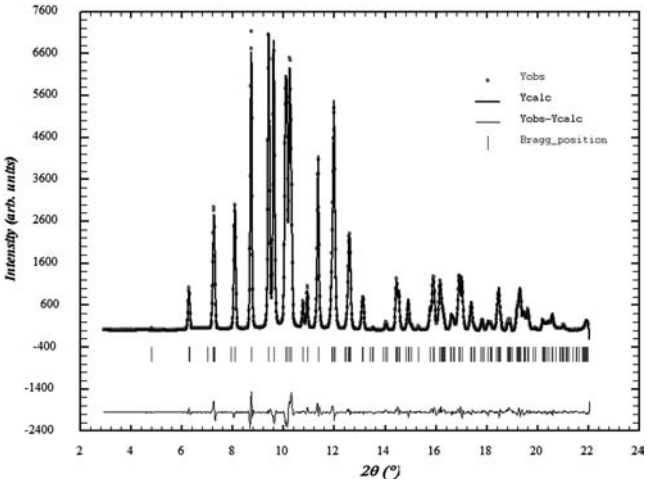

Figure 3. Observed, calculated, and difference X-ray diffraction profiles for the LP phase of Ag_2S at 3.2 GPa. Vertical markers indicate Bragg reflections of the initial $P2_1/n$ monoclinic structure. The R_{Bragg}, R_{wp} and R_p residuals, whose definitions are given in the FULLPROF manual,[18] are 0.0248, 0.0735, and 0.0539.

The values of the bulk modulus (B_0) and cell volume at zero pressure (V_0) are left to vary freely, and the first derivative with pressure B'_0 is fixed to 5.2 (to be better compared with theoretical results collected in section 3.4). The obtained characteristic parameters for the $P2_12_12_1$ phase are V_0 = 217.2(2) Å^3 and B_0 = 82(2) GPa.

3.3. Second Pressure-Driven Phase Transition. This HP1 phase is stable up to 10.5 GPa, where another transition takes place. At this point, the HP2 phase starts to appear (onset of the phase transition) and the peaks corresponding to the HP1 phase gradually lose intensity. There exists a region of coexistence of both phases between this pressure and 14 GPa, where the transition seems to be complete. The diffractograms above this pressure were of relatively poor quality, even the synchrotron data, and hindered a clear indexation of the Bragg reflections. Note that the diffraction peaks broaden noticeably above 8−9 GPa. Nevertheless, theoretical calculations came to our aid and suggested the monoclinic structure $P2_1/n$ with a β angle close to 94° (see Table 1 and the next section, devoted to theoretical simulations) as a possible structural candidate. With this in mind, we could index the XRD pattern at 16.5 GPa on the basis of a monoclinic cell with the following lattice parameters: a = 4.0939(12) Å, b = 5.754(2) Å, c = 7.9747(11) Å, and β = 93.87(2)° (Z = 4, V = 187.4(2) Å^3). The intensities of the diffraction peaks corresponding to the structural model proposed by theoretical simulations were not far away from those experimentally observed, which is why we carried out a Rietveld refinement of the limited-quality XRD pattern at 16.5 GPa. This X-ray diffraction pattern is shown in Figure 7 together with the calculated and difference profiles to illustrate

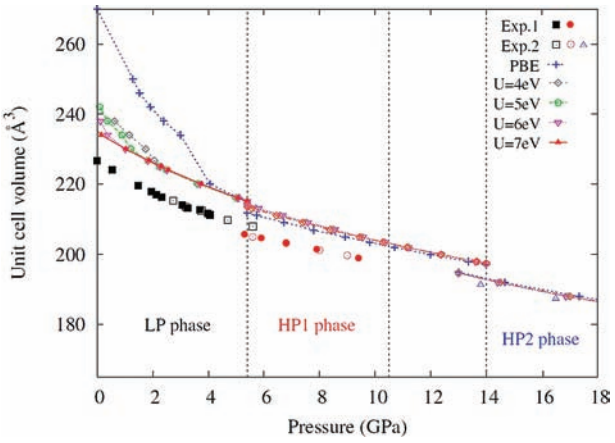

Figure 4. Pressure dependence of the unit-cell volume for the three phases of Ag_2S. Xcalibur (experiment 1) and Diamond (experiment 2) experimental data are represented by solid and empty symbols, respectively. Squares, circles, and triangles correspond to the LP, HP1, and HP2 phases, respectively. Calculated data using the PBE functional and the GGA+U approach, with U values of 7, 6, 5, and 4 eV are represented by points with lines. Dashed lines indicate the phase boundaries. The region between 10.5 and 14 GPa is the coexistence region of the HP1 and HP2 phases.

Table 1. Experimental and Calculated PBE Lattice Parameters, Volumes, and Fractional Coordinates of Ag_2S in the Low-Pressure (LP) Acanthite Phase (Anti-$PbCl_2$-Like Structure), in the First Pressure-Induced Phase HP1 (Ag_2Se-Type Structure), and in the Second Pressure-Induced Phase HP2[a]

	LP phase (4.7 GPa)		HP1 phase (6.9 GPa)		HP2 phase (16.5 GPa)	
	expt	theory	expt	theory	expt	theory
space group (No.)	$P2_1/n$ (14)	$P2_1/n$	$P2_12_12_1$ (19)	$P2_12_12_1$	$P2_1/n$ (14)	$P2_1/n$
a (Å)	4.1032(4)	4.2329	6.7249(12)	6.7791	4.0920(8)	4.1277
b (Å)	6.6391(6)	6.8078	4.1479(12)	4.3259	5.7519(13)	5.7278
c (Å)	7.8183(7)	7.7259	7.2945(11)	7.1154	7.9702(17)	8.0343
β (deg)	99.480(5)	102.45			93.819(15)	94.810
V (Å^3)	210.07(4)	217.4	203.48(8)	208.7	187.18(7)	189.3
x_{Ag1}	0.7419(9)	0.7634	0.0285(7)	0.0234	0.7402(9)	0.7331
y_{Ag1}	0.0277(5)	0.0214	0.2303(12)	0,241	0.0326(6)	0.0596
z_{Ag1}	0.3271(4)	0.3313	0.4079(14)	0.392	0.2921(3)	0.2843
x_{Ag2}	0.2476(8)	0.2471	0.1274(6)	0.1371	0.2564(9)	0.2545
y_{Ag2}	0.3440(5)	0.3452	0.4074(19)	0.401	0.2962(5)	0.3362
z_{Ag2}	0.4427(4)	0.4548	0.8210(6)	0.7886	0.4303(4)	0.4373
x_S	0.324(2)	0.3396	0.221(2)	0.2539	0.224(2)	0.2825
y_S	0.2608(13)	0.2426	0.157(4)	0.1313	0.266(2)	0.3013
z_S	0.1365(12)	0.1501	0.145(4)	0.0897	0.1068(12)	0.1133

[a]The three phases present four formula units per cell.

dx.doi.org/10.1021/ic300236p | Inorg. Chem. 2012, 51, 5289−5298

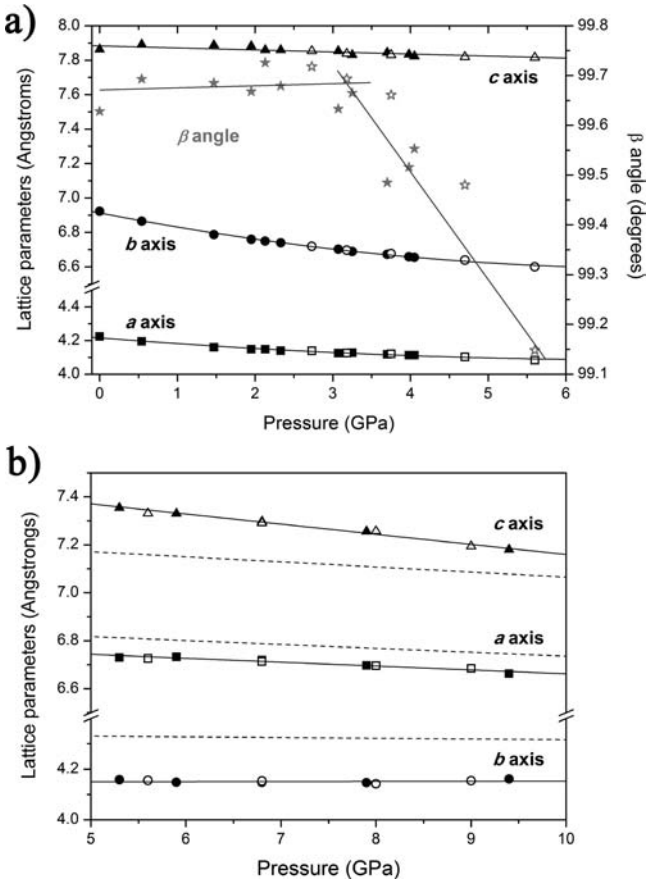

Figure 5. Evolution of the lattice parameters of the low-pressure (a) and the HP1 (b) phases of Ag_2S with pressure according to our experimental (Xcalibur, solid symbols; Diamond, empty symbols) and ab initio PBE data (dashed lines, see text). The *a*, *b*, and *c* axes are represented by squares, circles, and triangles, respectively. The β angle of the LP phase is represented by stars (Figure 5a). Solid lines correspond to second-order polynomial (a) and linear (b) fittings to our experimental data.

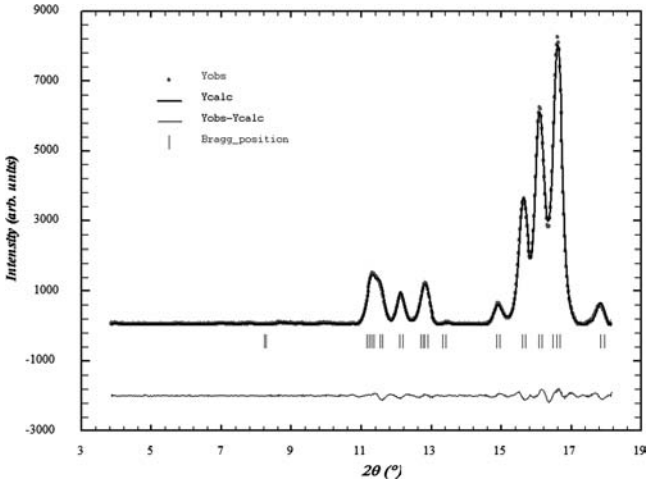

Figure 6. Observed, calculated, and difference X-ray diffraction profiles of the orthorhombic $P2_12_12_1$ phase of Ag_2S at 6.9 GPa (HP1 phase). The R_{Bragg}, R_{wp}, and R_p residuals are 0.0146, 0.069, and 0.0458.

the quality of the refinement. Taking into consideration the limitations of this refinement, we managed to obtain some tentative atomic coordinates for the HP2 phase. Both the refined lattice and atomic parameters are in good agreement with those theoretically calculated (see Table 1).

Table 2. Ag−S Bond Lengths (Å) in the LP $P2_1/n$ Anticotunnite-Like (P = 4.7 GPa), the HP1 $P2_12_12_1$ Ag_2Se-Type (P = 6.9 GPa), and the HP2 $P2_1/n$ Co_2Si-Like (P = 16.5 GPa) Phases

P = 4.7 GPa Anti-$PbCl_2$-like structure	P = 6.9 GPa Ag_2Se-type structure	P = 16.5 GPa Co_2Si-like structure
1 × 2.489	1 × 2.334	1 × 2.326
1 × 2.547	1 × 2.44	1 × 2.579
1 × 2.555	1 × 2.469	1 × 2.61
1 × 2.593	1 × 2.657	1 × 2.695
1 × 2.66	1 × 2.757	1 × 2.72
1 × 2.748	1 × 2.858	1 × 2.752
1 × 2.833	1 × 2.90	1 × 2.768
1 × 3.018	1 × 2.936	1 × 2.834
1 × 3.414	1 × 3.505	1 × 2.88
		1 × 3.066

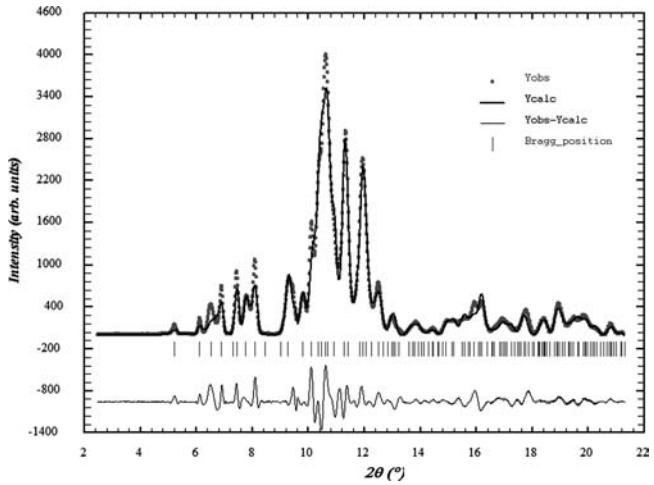

Figure 7. Observed, calculated, and difference X-ray diffraction profiles for the HP2 phase of Ag_2S at 16.5 GPa. Vertical markers indicate Bragg reflections of the high-pressure $P2_1/n$ monoclinic structure. The R_{Bragg}, R_{wp}, and R_p residuals are 0.0569, 0.124, and 0.111.

This HP2 structure is represented in Figure 2e, together with the other two phases of Ag_2S. It can be seen that the HP2 phase is a subtle variation of the initial monoclinic phase, the only difference being that the bases of the trigonal prisms are now almost equilateral triangles with edges of 2.916, 2.961, and 3.061 Å and angles of 57.91, 59.32, and 62.77° (as compared to edges of 3.13, 3.148, and 3.575 Å and angles of 55.04, 55.53, and 69.43° at room pressure). In spite of the minor changes in the structural topology, the coordination number of the S atoms increases from 8 + 1 in the initial anticotunnite-like structure to 10 in this HP2 structure. Table 2 collects the principal Ag−S distances of these two phases. The HP2 phase can be then considered as a Co_2Si-related structure. Cotunnite-type and Co_2Si-type structures described in the orthorhombic *Pnam* setting have been shown to exhibit characteristic values for the cell constant ratios a/b and $(a + b)/c$,[31−33] which are respectively 0.8−0.9, 3.3−4.0 and 0.66−0.74, 3.1−3.3. Despite the fact that our structures can only be described with a monoclinic $P2_1/n$ symmetry, if we calculate the b/c and $(b + c)/a$ ratios, we obtain values of 0.849, 3.523 and 0.722, 3.353 for the LP (4.7 GPa) and HP2 (16.5 GPa) phases, respectively.

dx.doi.org/10.1021/ic300236p | Inorg. Chem. 2012, 51, 5289−5298

These values would be in reasonable agreement with anticotunnite- and Co_2Si-type structures.

It is noteworthy that the initial monoclinic phase is fully recovered after decompression, the reversibility being observed in both experiments. The lattice parameters of the recovered sample are almost identical with those of the sample prior to compression: a = 4.2274(4) Å, b = 6.9246(5) Å, c = 7.8688(7) Å, and β = 99.661(6)° (V = 227.08(4) Å^3). Another important fact to note is that the HP1 phase was not observed in the only downstroke XRD measurement. The sample was measured at 6.8 GPa, and the powder diffractogram could be perfectly indexed into a monoclinic unit cell with constants a = 4.1393(11) Å, b = 6.097(2) Å, c = 7.9214(15) Å, and β = 96.68(2)° (V = 198.5(2) Å^3). Note that these values are just between those of the initial room-pressure phase and the HP2 phase at 16.5 GPa, both with the same space group, $P2_1/n$. This fact supports the argument of structures being very close energetically (LP and HP1) and show the existence of a possible stepwise transformation path from the HP2 to the LP phase. However, one decompression point is not enough to draw any conclusion and the indexed monoclinic phase could be also due to a hysteresis effect.

3.4. First-Principles Structural Study of Ag_2S. Calculated structural parameters for the different phases under the PBE approximation are given in Table 1, along with the experimental parameters. For the LP phase, a reasonable agreement is found between theory and experiment at 4.7 GPa. The calculated volume is overestimated by 3.7% with respect to the experimental value as a consequence of 3.4% and 2.6% larger a and b axes. An overestimation of volume is typical when using the GGA approximation.[34]

At pressures lower than 4 GPa there is an anomalous increase of the cell volume (see Figure 4). It can be related to an increase of symmetry of the pseudo-orthorhombic cell (space group $P2_1/n$), which finally converts into an orthorhombic cell (space group *Cmcm*) at low pressure. The equilibrium cell volume of this new phase is 270 Å^3, with a = 4.6406 Å, b = 7.3683 Å, c = 7.8963 Å and Ag(4*b*) (0, $^1/_2$, 0), Ag(4*c*) (0, 0.0520, $^1/_4$), S(4*c*) (0, 0.689, $^1/_4$). As far as we know, this orthorhombic phase has not been detected previously. Since its equilibrium volume is clearly larger than the experimental ambient-pressure volume of the anticotunnite-like structure, it could correspond to a potential high-temperature phase of Ag_2S. In fact, this new theoretically predicted phase adopts a Ni_2In-type related structure (*Cmcm* is a subgroup of $P6_3/mmc$, space group of the Ni_2In compound), which is very common among the alkali-metal sulfides. It basically consists of S-off-centered trigonal [Ag_6] prisms similar to those present in the anticotunnite structure, but now forming straight chains along the c direction (see Figure 2f).

From the enthalpy−pressure curves (Figure 8), two phase transitions are found. As a first step, the low-pressure phase transforms into the Ag_2Se-type structure at 3.25 GPa, with a volume change of 2.9%. This is in good agreement with the experimental data, where the onset of the phase transition was observed at 5 GPa. Calculated structural data of the HP1 phase at 6.9 GPa are collected in Table 1, to be compared with the experimental data. As described above, the coordination numbers of both the silver and the sulfur atoms do not change with increasing pressure. These numbers remain constant: Ag1, Ag2, and S atoms having 5, 4, and 9 nearest neighbors, respectively. However, the relative movement of the different polyhedra led to a slight change in the environment of all the

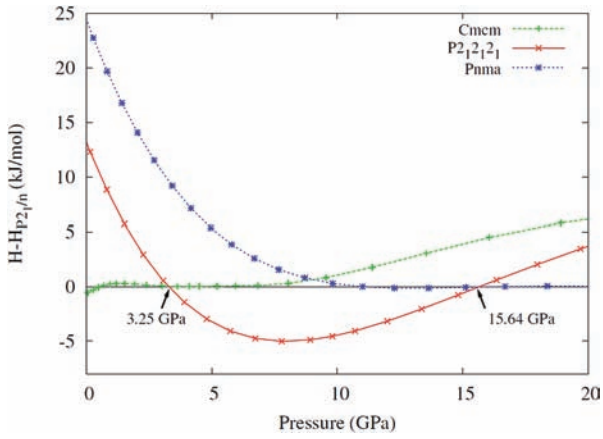

Figure 8. Enthalpy differences, relative to the $P2_1/n$ structure, as a function of pressure for the *Cmcm*, $P2_12_12_1$, and *Pnma* structures of Ag_2S. Calculations were performed at the PBE level.

atoms and, consequently, to the phase transition. Furthermore, a numerical equation of state was fitted to our data, giving the following parameters: V_0 = 225.57 Å^3, B_0 = 74.27 GPa and B_0' = 5.24. By comparing these results with those obtained from the fitting of the experimental data, we can see that the overestimation of volume by 3.9% leads to a slightly smaller bulk modulus.

With regard to the second phase transition, the calculations (Figure 8) show the reappearance of the monoclinic structure at higher pressures (15.64 GPa). According to the ab initio calculations, this monoclinic phase has suffered some significant changes in its unit cell, such as a drastic decrease of the b axis and the β angle and a considerable increase of the c axis. This effect can be clearly noticed by comparing the lattice parameters and atomic coordinates of the low-pressure and HP2 structures in Table 1. This behavior was subsequently confirmed experimentally by means of the indexation and refinement of the XRD pattern at 16.5 GPa (see section 3.3). A more careful analysis of the structural parameters of this HP2 structure shows a close resemblance to a higher symmetry structure (space group *Pnma*). At 16.7 GPa, a = 5.7411 Å, b = 4.0443 Å, c = 8.0971 Å, Ag(4*c*) (0.0689, 0.75, 0.7807), Ag(4*c*) (0.3435, 0.25, 0.9337), and S(4*c*) (0.3068, 0.25, 0.6104). As can be discerned from the relative enthalpy−pressure curves (Figure 8), the enthalpy of the *Pnma* structure equals that of the monoclinic structure at high pressures, confirming this fact. However, experimentally, a better fitting has been found using the monoclinic symmetry. The numerical equation of state parameters of the HP2 structure under the *Pnma* symmetry are V_0 = 223.66 Å^3, B_0 = 57.04 GPa, and B_0' = 7.85. Overall, the range of stability of the monoclinic phase is underestimated in comparison with the experimental results.

Phase diagrams more consistent with the experimental data can be obtained by the DFT+U approach. Although the experimentally unobserved *Cmcm* and *Pnma* phases are still present in the phase sequence, the range of stability of the monoclinic phase increases with growing U_{eff} value, showing the importance of the inclusion of correlation effects. Related to this, the HP1 structure is stable in a smaller pressure range. For example, when U_{eff} = 6 eV (Figure 9) the orthorhombic phase is only stable from 3.7 to 8.23 GPa, in comparison with the larger PBE pressure range (3.25−15.64 GPa). A reasonable structural description of the monoclinic structure is also obtained at pressures lower than 4 GPa (in particular, with

dx.doi.org/10.1021/ic300236p | *Inorg. Chem.* 2012, 51, 5289−5298

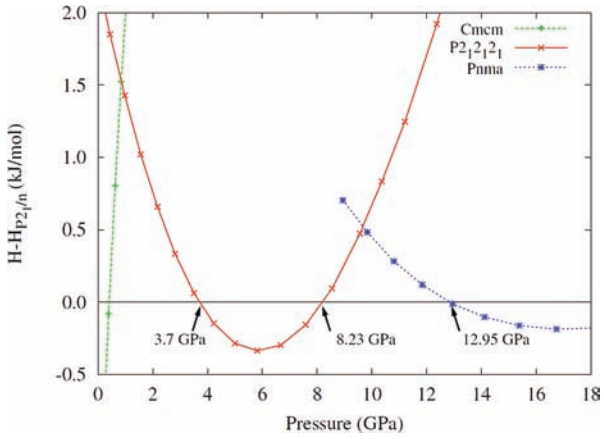

Figure 9. Enthalpy differences, relative to the $P2_1/n$ structure, as a function of pressure for the *Cmcm*, $P2_12_12_1$, and *Pnma* structures of Ag_2S. Calculations were performed at the GGA+U level, with U = 6 eV.

U_{eff} = 5−7 eV), as shown in Figures 4 and 10. With U_{eff} = 6 eV, the relative contractions of the lattice parameters *a*, *b*, and *c*

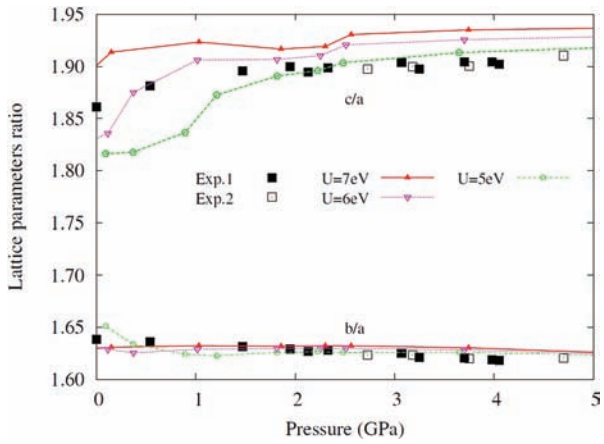

Figure 10. Lattice parameters ratios b/a and c/a as a function of pressure for the low-pressure phase (LP). Experimental data are represented by solid (experiment 1, Xcalibur) and open (experiment 2, Diamond) squares. Calculated data using the GGA+U approach, with U values of 7, 6, and 5 eV, are represented by points with lines.

between ambient pressure and 4.7 GPa are 4.84, 5.18, and −0.21%, in agreement with the experimental compressibility order (see section 3.1). Additionally, there is a recovery of the monoclinic phase after the orthorhombic phase, in line with the experimental results. Concerning the HP1 phase, there is an increase of the cell volume with growing U_{eff}. The volume is already overestimated at the purely GGA level (U_{eff} = 0). Thus, introducing U_{eff} > 0 just makes the deviation from the experiment larger. However, it equalizes the difference with experiment in all three vectors and the overall description of the cell improves, as the b/a and c/a ratios show (Figure 11).

3.5. Structural Considerations. According to our high-pressure experimental (theoretical) study, the structural sequence of Ag_2S with increasing pressure is as follows: anti-$PbCl_2$-like, LP, $P2_1/n$; Ag_2Se-type, HP1, $P2_12_12_1$; Co_2Si-like, HP2, $P2_1/n$; (Co_2Si-type, *Pnma*). Analyzing the atomic rearrangements, we note the following (i) This sequence does not correspond to those observed in alkali-metal sulfides under compression, where

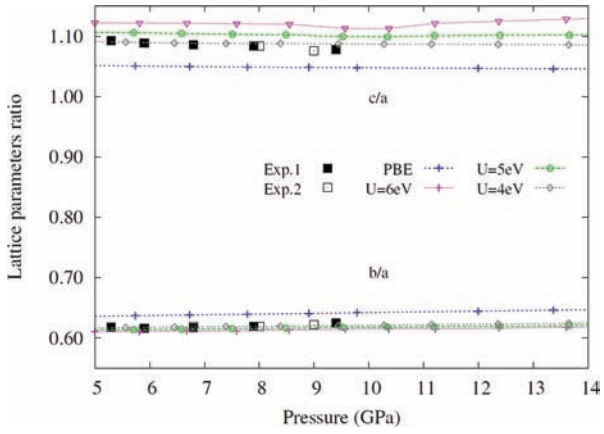

Figure 11. Lattice parameters ratios b/a and c/a as a function of pressure for the HP1 phase. Experimental data are represented by solid (experiment 1, Xcalibur) and open (experiment 2, Diamond) squares. Calculated data using the PBE functional and the GGA+U approach, with U values of 6, 5, and 4 eV, are represented by points with lines.

the anti-$PbCl_2$-type structure transforms into the Ni_2In-type structure.[10] This distinguishing structural behavior could be related to the high electronegativity value of silver, in comparison to that of alkali metals. However, in nature, there exist several examples where the anti-$PbCl_2$ → Ni_2In sequence is inverted,[35] which would imply that the existence of these phases might be restricted to a relatively small range in the P-T space. On top of that, the chemical bonds in alkali-metal sulfides could present a higher covalent character at high densities and then the structural sequence of all the M_2S compounds could converge at high pressures. These controversial points remain as open questions. (ii) The first phase transition LP−HP1 in Ag_2S follows the well-known trend that the high-pressure structures of lighter elements (S in Ag_2S) adopt the structures of their parent heavier elements on going down a column in the periodic table (Se in Ag_2Se).[36] (iii) Upon further compression, the Ag_2Se-type structure, with tilted chains of [Ag_6] prisms, transforms into the Co_2Si-like structure with a much more regular conformation than the initial anticotunnite-like structure, eventually adopting an orthorhombic space group in the theoretical calculations. In summary, in this article we have studied the pressure effects on the Ag_2S lattice, which add up to previous data on the behavior of this compound at high temperature. However, new experiments combining high pressure and high temperature would go into greater depth into the role played by these two thermodynamic variables in lattice modifications.

It is also interesting to compare the different Ag_2S polymorphs with the cation subarrays of their corresponding oxides. The Ag_2S subarray of Ag_2SO_3 (space group $P2_1/c$)[37] also adopts an anticotunnite-like structure, as in Ag_2S itself under room conditions. In this case, [Ag_6] prisms have expanded due to the presence of three O atoms per formula unit and form slightly warped chains. This case of structural similarity is in good agreement with numerous other examples of structural correspondence between alloys and the cation arrays in their oxides.[38−40] On the other hand, Ag_2SO_4 (like Ag_2SeO_4) adopts a thenardite-type (space group *Fddd*) structure,[41] whose cation subarray does not correspond to any of the high-pressure polymorphs of the silver sulfide. The cation arrangement in this oxide is similar to that of the $TiSi_2$ alloy. This structure was however predicted for Rb_2S at about 18 GPa[11] and has been

dx.doi.org/10.1021/ic300236p | Inorg. Chem. 2012, 51, 5289−5298

considered as the intermediate step in the Ni_2In-Cu_2Mg transition in the high-pressure sequence of the A_2X compounds.[35] In other words, the structure of the cation subarray of Ag_2SO_4 could be a potential structure for Ag_2S at still higher pressures.

4. CONCLUSIONS

The high-pressure structural stability of acanthite, Ag_2S, has been studied by means of X-ray diffraction experiments as well as by ab initio calculations. From our experimental data, we have determined that two different high-pressure phase transitions take place. At 5 GPa, the initial anti-$PbCl_2$-like monoclinic structure (space group $P2_1/n$) transforms into an orthorhombic Ag_2Se-type structure (space group $P2_12_12_1$), which is a strong distortion of the initial phase. The compression of the initial $P2_1/n$ structure is rather anisotropic, and the experimental values of the bulk modulus and its first derivative with pressure are B_0 = 38(2) GPa and B'_0 = 12(2). The characteristic parameters of the $P2_12_12_1$ HP1 structure obtained by fixing B'_0 to 5.2 are V_0 = 217.2(2) Å^3 and B_0 = 84(2) GPa (theory: V_0 = 225.57(3) Å^3, B_0 = 74.27(7) GPa, and B'_0 = 5.24(1)).

We have also found that compression induces a second phase transition at 10.5 GPa to a $P2_1/n$ phase which resembles the room-conditions structure. This HP2 monoclinic phase presents some significant changes in its unit cell with respect to the initial phase, such as a drastic decrease of the b axis and the β angle and a considerable increase in the c axis. This phase can be considered as a Co_2Si-related structure. It is noteworthy that the initial monoclinic phase is fully recovered after decompression.

Ab initio calculations confirm the experimental high-pressure sequence LP−HP1−HP2. Some deficiencies are found using standard DFT for modeling the electronic structure, but the GGA+U approach, with U_{eff} = 4−6 eV, is seen to perform better. A good agreement with experiment for transition pressures, lattice parameters, and their variation with pressure is found. Additionally, HP2 is predicted to transform to a *Pnma* structure at higher pressures. This should be confirmed experimentally. In summary, we have presented a detailed and consistent experimental and theoretical picture of the high-pressure behavior of Ag_2S.

■ ASSOCIATED CONTENT

Ⓢ Supporting Information

CIF files giving data for the crystal structures given in this study. This material is available free of charge via the Internet at http://pubs.acs.org.

■ AUTHOR INFORMATION

Corresponding Author

*E-mail: dsantamaria@quim.ucm.es.

Notes

The authors declare no competing financial interest.

⊥MALTA Consolider Team.

■ ACKNOWLEDGMENTS

Financial support from the Spanish Consolider Ingenio 2010 Program (Project No. CDS2007-00045) is acknowledged. The work was also supported by the Spanish MICCIN under Projects No. CTQ2009-14596-C02-01/02 and MAT2010-21270-C04-01, as well as from Comunidad de Madrid and European Social Fund: S2009/PPQ-1551 4161893 (QUIMAPRES). The Diamond Light Source is also acknowledged for provision of beamtime. O.G. acknowledges financial support from the Vicerrectorado de Investigación y Desarrollo de la UPV (Grants PAID-06-11 and PAID-05-11 through projects UPV2012-1469 and UPV2012-2682, respectively). M.M. is also grateful to the Principado de Asturias and FICYT for a Clarín postdoctoral fellowship (POST 10-54).

■ REFERENCES

(1) Frueh, A. J. *Acta Crystallogr.* **1957**, *10*, 764−764.
(2) Terabe, K.; Hasegawa, T.; Nakayama, T.; Aono, M. *Nature* **2005**, *433*, 47−50.
(3) Morales-Masis, M.; Van der Molen, S. J.; Fu, W. T.; Hesselberth, M. B.; Van Ruitenbeek, J. M. *Nanotechnology* **2009**, *20*, 095710.
(4) Rahlfs, P. *Z. Phys. Chem., Abt. B* **1936**, *31*, 157−194.
(5) Cava, R. J.; Reidinger, F.; Wuensch, B. J. *J. Solid State Chem.* **1980**, *31*, 69−80.
(6) Grier, B. H.; Shapiro, S. M.; Cava, R. J. *Phys. Rev. B* **1984**, *29*, 3810−3814.
(7) Blanton, T.; Misture, S.; Dontula, N.; Zdzieszynski, S. *Powder Diffr.* **2011**, *26*, 114−118.
(8) Grzechnik, A.; Vegas, A.; Syassen, K.; Loa, I.; Hanfland, M.; Jansen, M. *J. Solid State Chem.* **2000**, *154*, 603−611.
(9) Santamaria-Perez, D.; Vegas, A.; Muehle, C.; Jansen, M. *Acta Crystallogr., Sect. B* **2011**, *B67*, 109−115.
(10) Santamaria-Perez, D.; Vegas, A.; Muehle, C.; Jansen, M. *J. Chem. Phys.* **2011**, *135*, 054511.
(11) Schön, J. C.; Cancarevic, Z.; Jansen, M. *J. Chem. Phys.* **2004**, *121*, 2289−2304.
(12) Vegas, A.; Grzechnik, A.; Hanfland, M.; Muhle, C.; Jansen, M. *Solid State Sci.* **2002**, *4*, 1077−1081.
(13) Vegas, A.; Grzechnik, A.; Syassen, K.; Loa, I.; Hanfland, M.; Jansen, M. *Acta Crystallogr., Sect. B* **2001**, *57*, 151−156.
(14) Pauling, L. *J. Am. Chem. Soc.* **1932**, *54*, 3570−3582.
(15) Errandonea, D.; Santamaría-Pérez, D.; Bondarenko, T.; Khyzhun, O. *Mater. Res. Bull.* **2010**, *45*, 1732−1735.
(16) Hammersley, A. P.; Svensson, S. O.; Hanfland, M.; Fitch, A. N.; Hausermann, D. *High Press. Res.* **1996**, *14*, 235−248.
(17) Mao, H. K.; Xu, J.; Bell, P. M. *J. Geophys. Res., (Solid Earth Planets)* **1986**, *91*, 4673−4676.
(18) Rodriguez-Carvajal, J. *Physica B* **1993**, *192*, 55−69.
(19) Nolze, G.; Kraus, W. *Powder Diffr.* **1998**, *13*, 256−259.
(20) Kresse, G.; Furthmuller, J. *Phys. Rev. B* **1996**, *54*, 11169−11186.
(21) Kresse, G.; Joubert, D. *Phys. Rev. B* **1999**, *59*, 1758−1775.
(22) Monkhorst, H. J.; Pack, J. D. *Phys. Rev. B* **1976**, *13*, 5188−5192.
(23) Perdew, J. P.; Burke, K.; Ernzerhof, M. *Phys. Rev. Lett.* **1996**, *77*, 3865−3868.
(24) Dudarev, S. L.; Botton, G. A.; Savrasov, S. Y.; Humphreys, C. J.; Sutton, A. P. *Phys. Rev. B* **1998**, *57*, 1505−1509.
(25) Blochl, P. E.; Jepsen, O.; Andersen, O. K. *Phys. Rev. B* **1994**, *49*, 16223−16233.
(26) Otero-de-la-Roza, A.; Abbasi-Pérez, D.; Luaña, V. *Comput. Phys. Commun.* **2011**, *182*, 2232−2248.
(27) O'Keeffe, M.; Hyde, B. G. *Struct. Bonding (Berlin)* **1985**, *61*, 77−144.
(28) Billetter, H.; Ruschewitz, U. *Z. Anorg. Allg. Chem.* **2008**, *634*, 241−246.
(29) Wiegers, G. A. *Am. Mineral.* **1971**, *56*, 1882−1888.
(30) Yu, J.; Yun, H. *Acta Crystallogr., Sect. E* **2011**, *67*, i45.
(31) Jeitschko, W. *Acta Crystallogr., Sect. B* **1968**, *24*, 930−934.
(32) Léger, J. M.; Haines, J.; Atouf, A.; Schulte, O.; Hull, S. *Phys. Rev. B* **1995**, *52*, 13247−13256.
(33) Haines, J.; Léger, J. M.; Schulte, O. *Phys. Rev. B* **1998**, *57*, 7551−7555.
(34) Haas, P.; Tran, F.; Blaha, P.; Schwarz, K. *Phys. Rev. B* **2011**, *83*, 205117.
(35) Vegas, A. *Struct. Bonding (Berlin)* **2011**, *138*, 133−198.

(36) Arroyo y de Dompablo, M. E.; Santamaria-Perez, D.; Persson, K. Polymorphs by Pressure In *High Pressure Processes in Chemical Engineering*; Verlag ProcessEng Engineering: Vienna, Austria, 2011.
(37) Larsson, L. O. *Acta Chem. Scand.* **1969**, *23*, 2261−2269.
(38) Vegas, A.; Jansen, M. *Acta Crystallogr., Sect. B* **2002**, *58*, 38−51.
(39) Santamaria-Perez, D.; Vegas, A.; Liebau, F. *Struct. Bonding (Berlin)* **2005**, *118*, 121−177.
(40) Santamaria-Perez, D., Chulia-Jordan, R. *High Press. Res.* **2011**, DOI: 10.1080/08957959.2011.635143
(41) Zachariasen, W. H. *Z. Kristallogr.* **1932**, *82*, 161−162.